Available online at www.sciencedirect.com
ScienceDirect
Ceramics International 36 (2010) 635–641
CERAMICS INTERNATIONAL
www.elsevier.com/locate/ceramint

Effects of niobium doping site and concentration on the phase structure and oxygen permeability of Nb-substituted $SrCoO_x$ oxides

Kun Zhang [a], Ran Ran [a], Zongping Shao [a,*], Zhonghua Zhu [b], Yonggang Jin [b], Shaomin Liu [c,*]

[a] State Key Laboratory of Materials-oriented Chemical Engineering, College of Chemistry & Chemical Engineering, Nanjing University of Technology, Nanjing 210009, PR China
[b] ARC Center for Functional Nanomaterials, School of Engineering, The University of Queensland, Brisbane, Queensland 4072, Australia
[c] Department of Chemical Engineering, Curtin University of Technology, Perth, WA 6845, Australia

Received 16 May 2009; received in revised form 1 September 2009; accepted 25 September 2009
Available online 29 October 2009

Abstract

Niobium doping effect on phase structure, phase stability and electrical conductivity of $SrCoO_x$ oxides and oxygen permeability of the corresponding membranes were systematically investigated. Niobium was successfully incorporated into A-site, B-site or simultaneously A and B double sites of $SrCoO_x$ oxide and stabilized the perovskite structure with a cubic symmetry in air down to room temperature at a proper doping amount. However, the A-site doping could not stabilize the cubic structure under a more reducing atmosphere of nitrogen, as to $SrCo_{1-y}Nb_yO_{3-\delta}$, $y \geq 0.1$ is necessary to sustain the cubic perovskite structure. Simultaneous doping of Nb at A and B sites is the most effective way to stabilize the perovskite structure under nitrogen atmosphere. Irrespective of doping site, the electrical conductivity decreased monotonously with Nb-doping amount. Both $Nb_xSr_{1-x}CoO_{3-\delta}$ and $Nb_zSr_{1-z}Co_{1-z}Nb_zO_{3-\delta}$ envisaged a decrease in oxygen permeation flux with Nb-doping amount while $SrCo_{1-y}Nb_yO_{3-\delta}$ reached the maximum flux at $y = 0.1$. Among all the membranes, $SrCo_{0.9}Nb_{0.1}O_{3-\delta}$ and $Nb_{0.05}Sr_{0.95}Co_{0.95}Nb_{0.05}O_{3-\delta}$ show the highest oxygen fluxes of 3.5 and 2.7 ml cm^{-2} min^{-1} at 900 °C under an air/helium gradient, respectively.

Keywords: Perovskite; $SrCoO_x$; Niobium; Ceramic membrane; Oxygen permeation; Conductivity

1. Introduction

Some oxides such as perovskite-structured $SrCo_{0.8}Fe_{0.2}O_{3-\delta}$ showing mixed oxygen ionic and electronic conductivity (MIEC) at elevated temperatures are currently attracting much research interest due to their potential use in air separation and membrane reactors for gas partial oxidations [1–9]. These perovskite-type oxides possess electronic conductivity higher than 1000 S cm^{-1} and oxygen ionic conductivity as high as 1 S cm^{-1} [10,11] at elevated temperatures. Such materials are also promising cathode candidates for intermediate-temperature solid-oxide fuel cells [12–14]. Compared to the traditional electrodes with pure electronic conductivity such as lanthanum strontium manganate, MIEC cathode effectively extends reaction sites for oxygen reduction from traditional electrolyte–electrode–air triple phase boundary to the entire cathode surface; therefore, a significant reduction in electrode polarization resistance is resulted [12–17].

Up to now, MIEC material development is still focused on these cobalt-based perovskites due to their high oxygen permeation fluxes, high catalytic activity for oxygen reduction and good ion diffusion properties [18,19]. Over the last several years, considerable efforts have been put on the further improvement of phase stability and oxygen permeability of cobalt-based oxides ($SrCoO_x$) via the doping strategy. It is well known that perovskite oxides are highly flexible in material composition and over 90% of atomic elements in the periodic table of elements can be incorporated inside the perovskite structure. Previously we demonstrated that $SrCoO_x$ can be stabilized into a cubic perovskite structure (ABO_3) when both A and B sites were simultaneously doped with a certain amount of yttrium [20]. The resultant membranes showed higher oxygen permeation fluxes and structural stability. Recently, niobium has been

* Corresponding authors. Tel.: +86 25 83172256/+61 8 92669056; fax: +86 25 83172256/+61 8 92662681.
E-mail addresses: shaozp@njut.edu.cn (Z. Shao), shaomin.liu@curtin.edu.au (S. Liu).

0272-8842/$36.00
doi:10.1016/j.ceramint.2009.09.040

reported to be one of the best B-site dopants for improving the phase structure and oxygen permeability [19,21]. In previous paper, we have systematic investigation of the Nb-doping into A-site of $SrCoO_x$ on its phase structure, phase stability, electrical conductivity and the oxygen permeation flux of the corresponding membranes [21]. In this paper, we showed further optimization of the material composition and the development of new $SrCoO_x$ based membranes doped by Nb at A-site or double A/B sites. The effects of doping site (A or A and B double sites) and Nb-doping concentration on the phase structure and oxygen permeability of the resulted MIEC membranes were systematically investigated and compared with the previous work of the B-site doped membrane [21].

2. Experimental

2.1. Synthesis and fabrication

Nb-doped $SrCoO_x$ oxides were synthesized by a solid-phase reaction with $SrCO_3$, Nb_2O_5 and Co_2O_3 (all in analytical grades) applied as the raw materials for the metal sources. Stoichiometric quantities of $SrCO_3$, Nb_2O_5 and Co_2O_3 (Sinopharm Chemical Reagent Co., Ltd, purity > 99.9%) had been mixed for 30 min using a FRITSCH Pullerisette 6 high-energy ball miller under acetone liquid media at a rotation speed of 500 RPM. After drying, the mixture was calcined at 1100–1200 °C in air for 10–20 h to form the oxides with desired structure.

The as-synthesized oxide powders were milled again by high-energy ball to get the qualified uniform powders, which was pressed into a disk-shaped membrane in a stainless steel mold (15 mm in diameter) under a hydraulic pressure of approximately 1.5×10^8 Pa. These green pellets were sintered in an electrical box furnace at 1100–1250 °C for 2–5 h in air at a heating/cooling rate of 1–2 °C min^{-1}.

2.2. Basic characterization

The crystal structure of the synthesized powders or sintered membranes was characterized by an X-ray diffractometer (XRD, Bruker D8 Advance) equipped with Cu Kα radiation. To examine the phase stability in a nitrogen atmosphere, the samples were put into a U-type quartz tube and treated at 850 °C in N_2 for 6 h. After the heat-treatment, the sample was cooled down to room temperature for phase examination.

The electrical conductivity was measured by four-probe dc method based on sintered bars of approximate dimensions 2 mm × 5 mm × 12 mm. The measurements were performed in air upon cooling from 900 to 300 °C with 5 °C/step. A constant current was applied to the two current wires and the voltage response on the two voltage wires was recorded using a Keithley 2420 sourcemeter. The current was increased from 1 μA to 2 A with the step of 1000 μm, only the data following the ohmic law were applied for the calculation of the conductivity.

2.3. Oxygen permeation measurement

Permeation properties of the membranes were investigated via a gas chromatography (GC) method using a high-temperature oxygen permeation apparatus [20]. A silver paste was used as the sealant to fix the membrane disk onto a dense quartz tube. The effective area for permeation study was around 0.45 cm^2. The ambient air was used as the feed gas and helium as the sweeping gas to carry the permeated oxygen to a Varian 3800 gas chromatography (GC) equipped with a 5 Å molecular sieve capillary column for in situ gas composition analysis. The temperatures for oxygen permeation measurement were arranged from 700 to 900 °C. Depending on the temperature, the measured oxygen concentration in outlet gases from the sweeping gas side was up to 2.6%. However, due to the leakage from the sealing area at high temperatures, nitrogen was also detected with a concentration up to 0.11%. Therefore, the oxygen flux value by mixed conduction was calculated by subtracting the amount of air leakage from the total flux values according to the method reported earlier [2].

3. Results and discussion

3.1. Phase structure

Shown in Fig. 1 are the X-ray diffraction patterns of A-site ($Nb_xSrCo_{1-x}O_{3-\delta}$) and double-site (A and B) Nb-doped $SrCoO_x$ oxides with composition of $(Nb_zSr_{1-z})(Co_{1-z}Nb_z)O_{3-\delta}$ where x, and z varies from 0.025 to 0.4. Niobium oxide phase (Nb_2O_5) was not observed in the diffraction patterns suggesting that niobium was successfully incorporated inside the perovskite structure of $SrCoO_x$ oxides. It is well known that the pristine parent material $SrCoO_x$ demonstrates a 2H hexagonal $BaNiO_3$-type structure, a distorted perovskite structure with oxygen vacancy ordered in its lattice resulting from the ionic size mismatch of A- and B-site cations [22]. Because of the immobilized oxygen in $SrCoO_x$ lattice, $SrCoO_x$ membrane exhibited a very small oxygen permeation flux near zero at temperatures lower than 900 °C [19,21,22].

A small amount of Nb-doping into one or both of A and B sites (x, y and $z = 0.025$) can effectively stabilize the lattice structure of the oxygen vacancy-disordered perovskite with cubic symmetry. Such cubic perovskite structure can be well sustained at Nb-doping concentration up to 0.2 for single site doping ($Sr_{1-x}Nb_xCoO_{3-\delta}$ or $SrCo_{1-y}Nb_yO_{3-\delta}$) on A or B and 0.1 for double-site doping ($Nb_zSr_{1-z}Co_{1-z}Nb_zO_{3-\delta}$), respectively. At doping concentration higher than these values, one additional diffraction peak with 2θ angle around 33° started to appear, indicating a phase transition from cubic perovskite to an oxygen vacancy-ordered brownmillerite-related phase structure at room temperature. For joint doping on both cites, when z value is over 0.2 (e.g., 0.4), three crystal phases of brownmillerite structure, cubic perovskite and $Co_{0.66}Nb_{1.33}O_4$ [JCPDS 75-2340] co-existed as shown in Fig. 1b. By the use of yttrium as the dopant, previously we found that $SrCoO_x$ cubic perovskite structure can only tolerate single A-cite doping or joint doping on both cites up to concentrations of 10% and 5%,

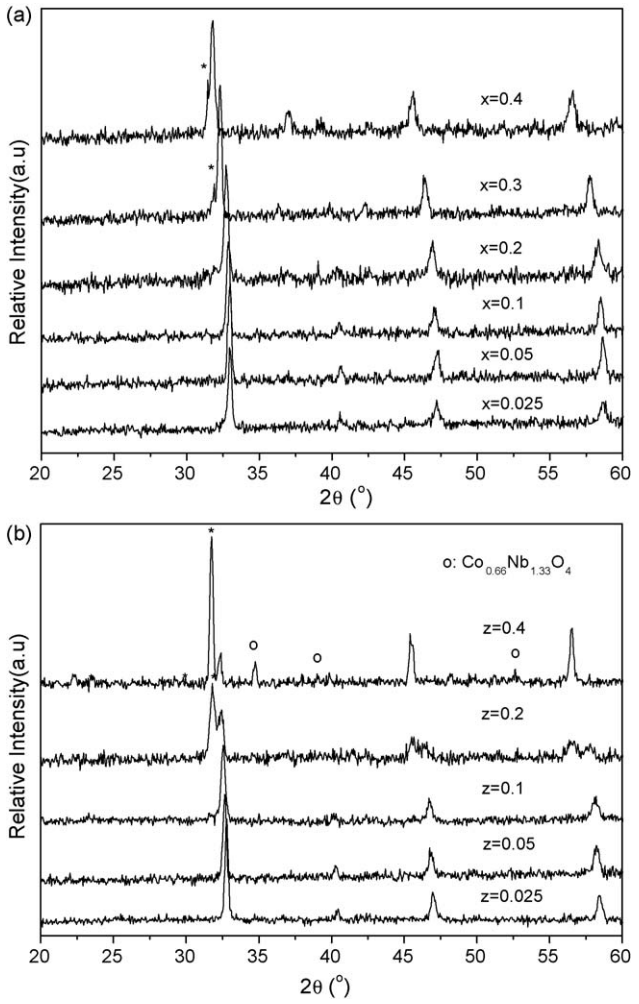

Fig. 1. Room-temperature X-ray diffraction patterns of oxides calcined at 1150 °C in air for 5 h: (a) $Nb_xSr_{1-x}CoO_{3-\delta}$, $x = 0.025$–0.4; (b) $Nb_zSr_{1-z}Co_{1-z}Nb_zO_{3-\delta}$, $z = 0.25$–0.4). (*) Non-cubic perovskite phase.

respectively [20]. Doping concentration directly affects the formed oxygen vacancy concentration of the resulted oxides, which further influences the material performance in oxygen separation. Compared to yttrium as the dopant, $SrCoO_x$ cubic perovskite can accept niobium dopant with a higher concentration. It was noted that the ionic radii of the dopants have effects on the structural stability of the doped compounds and also on the maximum level that the parent compounds can accept. For doping the ceria electrolyte, the dopant having ionic radius close to size of the ceria could give rise to a lower association enthalpy values with a more stable doping structure [23]. Nb^{5+}, Y^{3+} and Co^{3+} (HS) in six coordination with oxygen ions have an ionic radius of 0.64, 0.9 and 0.61 Å, respectively [24]. Thus, Nb^{5+} will have a better match than Y^{3+} with Co^{3+} because of their relative similar ionic radius in size. This may partially explain the wider doping range limit for Nb^{5+} than Y^{3+} as a dopant to stabilize the oxygen vacancy-disordered cubic perovskite structure.

Fig. 2 shows the magnified parts of the diffraction peaks of Nb-doped $SrCoO_x$ on three different circumstances. These peaks with 2θ around 33° can be indexed as the lattice plane peak of {1 1 0} of the cubic perovskite structure. As can be seen, the peaks were shifted to the lower angles with increasing Nb concentration for the doped samples with the lattice parameters showing in Table 1. The lattice parameter change implies that unit cell volumes of the resulted perovskite crystal phases are expanding with the increase of Nb concentration at A- or B-site. The cell expansion with Nb-doping amount at the B-site can be explained by the replacement of smaller ionic sized-cobalt ions (Co^{3+} and Co^{4+}) with larger sized-Nb^{5+}. The increase in unit cell volume of the A-site Nb-doped samples could be attributed to the increased average ionic radius of cobalt ions, regardless the fact that Nb^{5+} has a smaller ionic size than Sr^{2+}. The entrance of Nb^{5+} with a higher valence state than Sr^{2+} to the A-site facilitates the cobalt in the B-site to take a

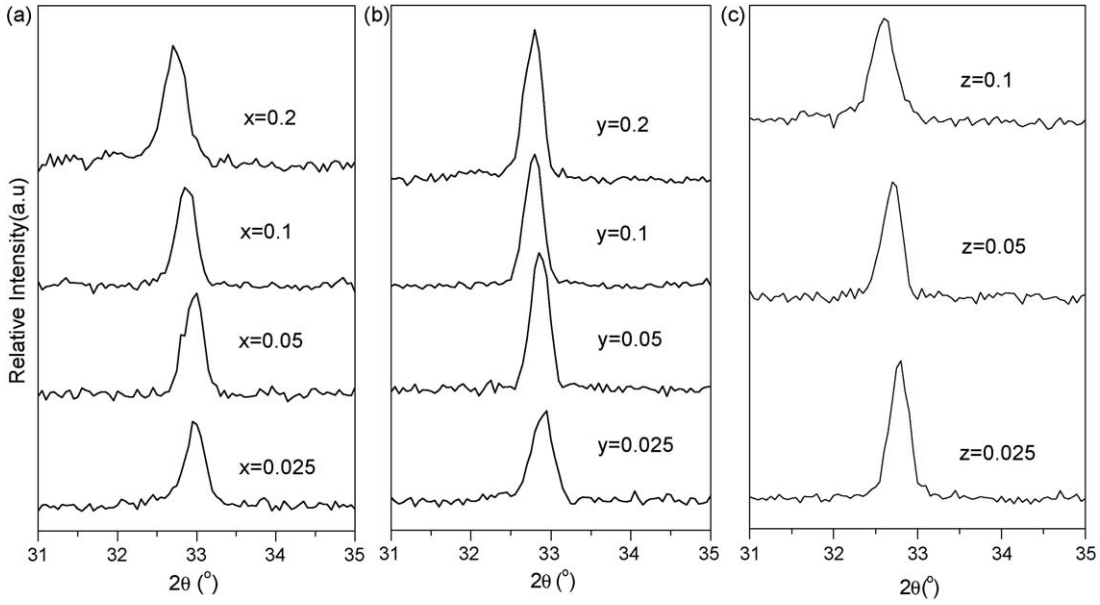

Fig. 2. The magnification of the diffraction peak of Nb-doped $SrCoO_x$ at around 33°: (a) $Nb_xSr_{1-x}CoO_{3-\delta}$, $x = 0.025$–0.2; (b) $SrCo_{1-y}Nb_yO_{3-\delta}$, $y = 0.025$–0.2; (c) $Nb_zSr_{1-z}Co_{1-z}Nb_zO_{3-\delta}$, $z = 0.25$–0.1.

Table 1
Lattice parameters of various Nb-doped $SrCoO_x$ oxides.

Composition	Space group	a (Å)	V (Å^3)
A-site			
$Nb_{0.025}Sr_{0.975}CoO_{3-\delta}$	*Pm3m*	3.846(4)	56.90(6)
$Nb_{0.05}Sr_{0.95}CoO_{3-\delta}$	*Pm3m*	3.851(2)	57.12(0)
$Nb_{0.1}Sr_{0.9}CoO_{3-\delta}$	*Pm3m*	3.861(5)	57.57(9)
$Nb_{0.2}Sr_{0.8}CoO_{3-\delta}$	*Pm3m*	3.870(8)	57.99(6)
A/B double sites			
$Nb_{0.025}Sr_{0.975}Co_{0.975}Nb_{0.025}O_{3-\delta}$	*Pm3m*	3.873(6)	58.12(2)
$Nb_{0.05}Sr_{0.95}Co_{0.95}Nb_{0.05}O_{3-\delta}$	*Pm3m*	3.874(2)	58.14(9)
$Nb_{0.1}Sr_{0.9}Co_{0.9}Nb_{0.1}O_{3-\delta}$	*Pm3m*	3.875(7)	58.21(7)

lower valence state, thus contributing the unit cell volume increase. For the same Nb-doping level, it is interesting to observe that the unit cell gets the biggest expansion when the Nb is distributed on two sites rather a single site. For example, for the same doping concentration with 5%, the unit cell volumes of $Nb_{0.05}Sr_{0.95}CoO_{3-\delta}$, $SrCo_{0.95}Nb_{0.05}O_{3-\delta}$ and $Nb_{0.025}Sr_{0.975}Co_{0.975}Nb_{0.025}O_{3-\delta}$ are 57.12, 57.42 and 58.12 Å^3, respectively. This phenomenon is attributable to the joint effects from A and B double-site doping.

To be used as a MIEC membrane for oxygen separation, the perovskite membrane must be exposed to asymmetric gas atmosphere conditions with different oxygen partial pressures on both sides. To ensure a stable oxygen permeation flux, the doped membranes have to possess sufficiently high phase stability under very low oxygen partial pressure or reducing atmosphere. It should be noted that these perovskite oxides are generally stable in air or other atmosphere containing a higher oxygen concentration. To examine their structural stability, the crystal phases of the doped $SrCoO_x$ samples under nitrogen atmosphere were investigated with results showing in Fig. 3. For single A-site doping, $Nb_xSr_{1-x}CoO_{3-\delta}$ samples with x values ranged from 0.025 to 0.20 having stable cubic perovskite phases in air exhibit the phase transition to an oxygen vacancy-ordered brownmillerite structure indicating the instability in nitrogen atmosphere. By contrast, the samples of $Nb_zSr_{1-z}Co_{1-z}Nb_zO_{3-\delta}$ with doping on both A/B cites display better structural stability as no any other phases were observed from their XRD patterns. This also demonstrates that the double-site doping is more effective to improve the stability of the cubic perovskite structure in reducing atmosphere. Similar results were observed from other research work by using Y^{3+} as the dopant [20].

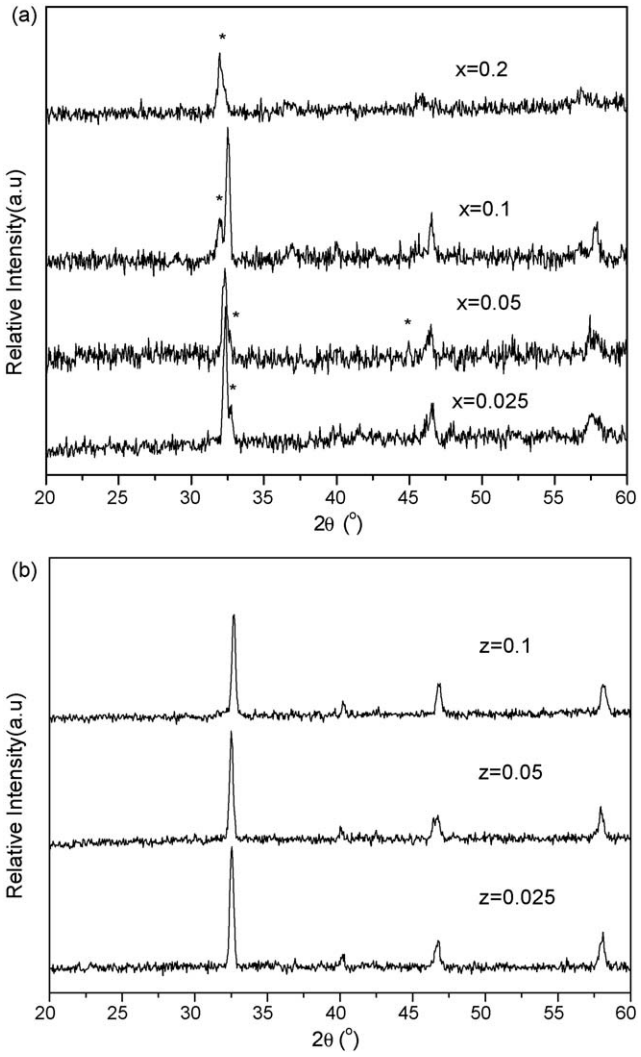

Fig. 3. Room-temperature X-ray diffraction patterns of oxides annealed at 850 °C under nitrogen atmosphere for 6 h: (a) $Nb_xSr_{1-x}CoO_{3-\delta}$, x = 0.025–0.2; (b) $Nb_zSr_{1-z}Co_{1-z}Nb_zO_{3-\delta}$, z = 0.25–0.1. (*) Non-cubic perovskite phase.

3.2. Electrical conductivity

Fig. 4 shows the temperature dependence of electrical conductivity of cubic perovskite-structured $Nb_xSr_{1-x}CoO_{3-\delta}$ (x = 0.025–0.2) and $Nb_zSr_{1-z}Co_{1-z}Nb_zO_{3-\delta}$ (z = 0.025–0.1) oxides in air. The corresponding data of $SrCo_{1-y}Nb_yO_{3-\delta}$ (y = 0.025–0.2) can be seen elsewhere [21]. For the three series of materials, a decrease in electrical conductivity with increasing Nb-doping amount was observed. As a whole, all the samples show metal-like conducting behavior at temperature higher than 500 °C, i.e., a decrease in electrical conductivity with increasing temperature.

It is well known that electrical conductivity is closely related to the phase structure and also the compositions and oxidation states of the compositional cations. The electron conduction in perovskite oxide proceeds via electron hopping along B-site cations through strong overlapping B–O–B bonds with a mechanism like the Zerner double exchange process as shown below [25]:

$$B^{n+}O^{2-}B^{(n+1)+} \Rightarrow B^{(n+1)+}O^{-}B^{(n+1)+} \Rightarrow B^{(n+1)+}O^{2-}B^{n+}$$

The overlapping of the 2p orbital of the oxygen ion with outer orbital of the transition cations (cobalt ions) results in the electron conduction. The higher degree of overlapping between the outer orbit of B-site ions and 2p orbit of oxygen ion and the easier redox of the B-site metal ions, the easier for the electron hopping, the higher electrical conductivity is expected. As demonstrated previously, the lattice constant increased with

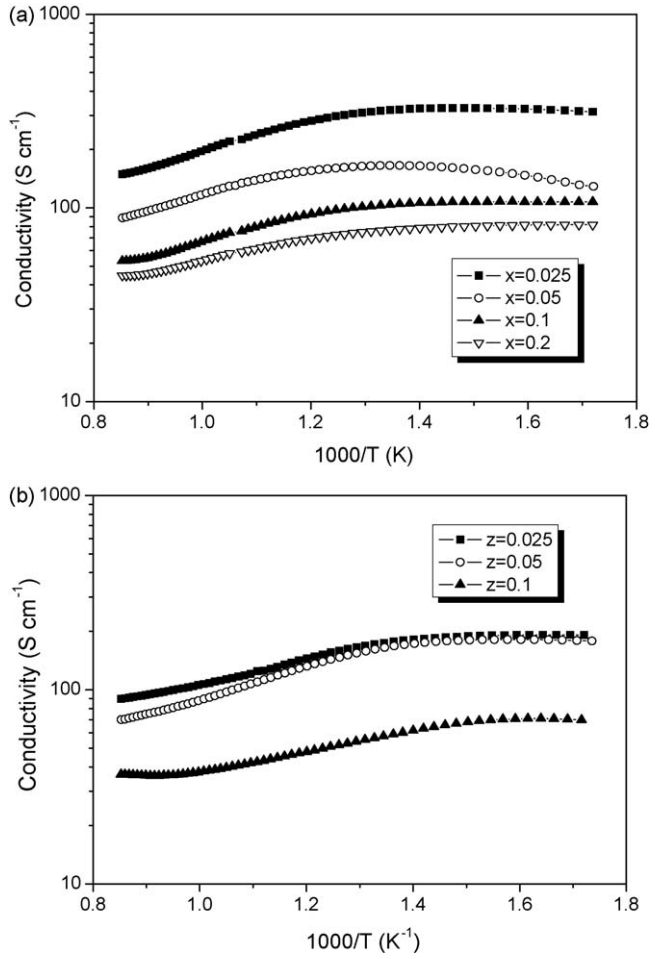

Fig. 4. Total electrical conductivity between 300 and 900 °C in air of: (a) $Nb_xSr_{1-x}CoO_{3-\delta}$, $x = 0.025$–0.2; (b) $Nb_zSr_{1-z}Co_{1-z}Nb_zO_{3-\delta}$, $z = 0.25$–0.1.

Nb-doping content in the A-site of $SrCoO_x$ [21]. It suggests the average oxidation state of cobalt ions was decreased with increasing Nb-doping concentration; it then led to a decrease of the electron density of the 3d orbit of cobalt. On the other hand, the increase in lattice constant also decreases the overlapping of cobalt 3d orbital and oxygen 2p orbital. Both factors lead to a decrease of electronic conductivity with increasing Nb-doping concentration at the A-site.

Since the oxidation state variation between Nb^{4+} and Nb^{5+} is much more difficult than that between Co^{3+} and Co^{4+}, Nb^{5+} perhaps acts as a block for electron hopping when it is doped into B-site of $SrCoO_x$. Consequently, the higher Nb^{5+} doping concentration the more difficult it is for the electrons to hop. Therefore, this could well explain the decreasing electrical conductivity with increasing Nb^{5+} doping concentration at the B-site. As to $Nb_zSr_{1-z}Co_{1-z}Nb_zO_{3-\delta}$, both effects may have contributed to the decrease in electrical conductivity with Nb-doping content.

3.3. Oxygen permeability

The oxides were fabricated into dense ceramic disks by dry pressing using a stainless steel die and sintered at 1200 °C for 5 h in air. The sintering density was measured by Archimedes method using water as the liquid media. All the sintered membranes were found to have a density higher than 93%. Microstructure of the ceramic membranes was also observed via SEM. All these membrane displays similar morphology with a typical one showing in Fig. 5 from A and B double-site Nb-doped $Nb_{0.025}Sr_{0.975}Co_{0.975}Nb_{0.025}O_{3-\delta}$ membranes. As can be seen, at this sintering condition, the grain size can be up to 10 μm. Gas leakage test at room temperature confirmed that there are no through pinholes inside the ceramic disks.

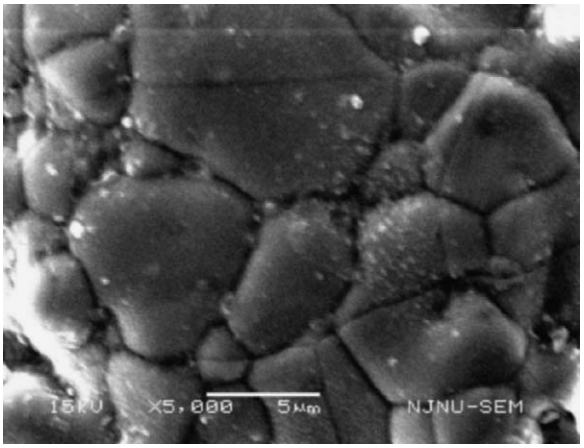

Fig. 5. SEM image of the sintered membrane from $Nb_{0.025}Sr_{0.975}Co_{0.975}Nb_{0.025}O_{3-\delta}$.

Both faces of the membranes polished by 1000 mesh SiC sand paper down to a uniform membrane thickness of 1.0 mm. The oxygen permeation fluxes of the membranes were measured at various temperatures by applying ambient air as the oxygen rich side atmosphere and a helium flow at 100 ml min^{-1} [STP]. Then it was introduced to another chamber to allow the sweep gas to create a medium level of oxygen gradient across the membrane. Fig. 6 shows the temperature dependence of oxygen permeation fluxes through the various membranes from A-site doping and A and B double-site doping. The permeation information of the membranes from B-site doping can be found in our previous work [21]. For the $SrCoO_{3-\delta}$ membrane without Nb-doping, a zero permeation flux was observed between 700 and 900 °C. As can be seen from Fig. 6, for both series of $Nb_xSr_{1-x}CoO_{3-\delta}$ and $Nb_zSr_{1-z}Co_{1-z}Nb_zO_{3-\delta}$ membranes, the permeation flux increases drastically with minor Nb-doping concentration up to 5%, and then decreases with the further increase of Nb-doping larger than 5%. While for B-site doped $SrCo_{1-y}Nb_yO_{3-\delta}$ membranes, the best Nb-doping concentration for achieving a maximum flux is 10% much larger than that of A-site or A and B double-site doped samples.

Under bulk diffusion controlling steps in the cases of most thick disk-shaped membranes, the oxygen permeation flux can be expressed by

$$J_{O_2} = -\frac{1}{4LV_m}\int_{\ln P'_{O_2}}^{\ln P''_{O_2}} C_v D_v \, \mathrm{d}\ln[p_{O_2}]$$

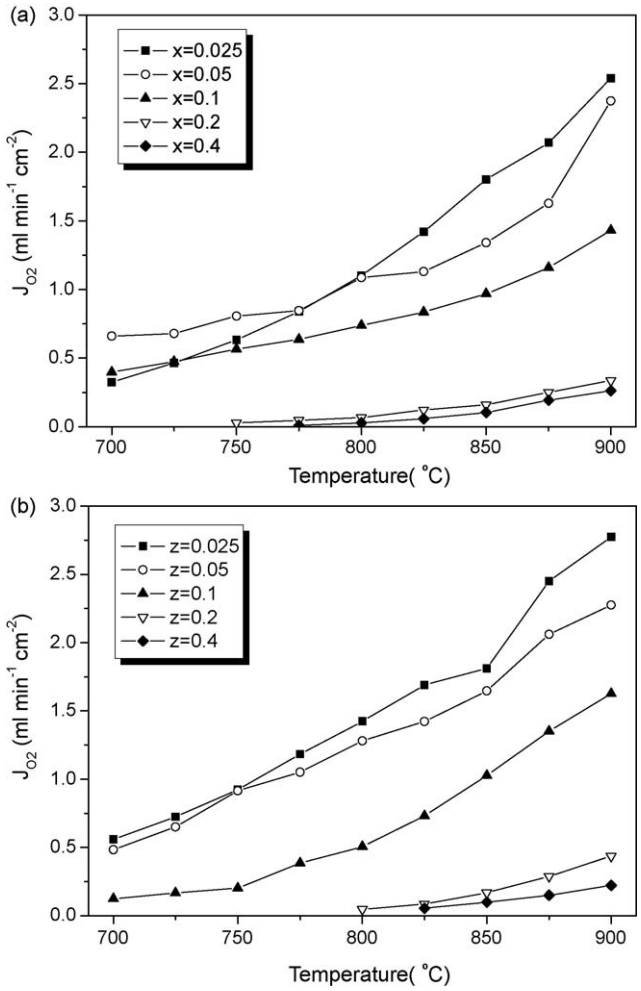

Fig. 6. The temperature dependence of oxygen permeation fluxes through: (a) $Nb_xSr_{1-x}CoO_{3-\delta}$, $x = 0.025$–0.4; (b) $Nb_zSr_{1-z}Co_{1-z}Nb_zO_{3-\delta}$, $z = 0.25$–0.4.

At a fixed membrane thickness, temperature and oxygen partial pressure gradient across the membrane, the oxygen permeation flux is determined by oxygen vacancy concentration (C_v) and oxygen bulk diffusion coefficient (D_v) of the membrane, which are closely related with the phase structure of the materials.

Cubic perovskite structure is an oxygen vacancy-disordered structure which ensures a high oxygen bulk diffusion rate. This is the reason for $Nb_xSr_{1-x}CoO_{3-\delta}$ and $Nb_zSr_{1-z}Co_{1-z}Nb_zO_3$ membranes to get a sharply improved oxygen fluxes with the initial lower Nb-doping concentration less than 5% which can stabilize the cubic perovskite structure. On the other hand, 2H hexagonal structure and oxygen vacancy-ordered brownmillerite structure have poor oxygen mobility. As discussed previously, A-site doped samples of $Nb_xSr_{1-x}CoO_{3-\delta}$ perovskites envisaged a decrease in phase stability of the oxygen vacancy-disordered cubic perovskite structure under lower oxygen containing atmosphere. Therefore, the oxygen diffusion in the membrane bulk near the helium sweep side membrane surface was likely suppressed with the introduction of Nb content. On the other hand, the increase of Nb content also reduced the oxygen vacancy concentration inside the oxide lattice since Nb^{5+} has higher valence state than Sr^{2+}. Both factors contributed to the decrease of the permeation flux with increasing Nb-doping content in the A-sited doped $Nb_xSr_{1-x}CoO_{3-\delta}$ membranes. Regarding the A and B double-site doping, the D_v can be reasonably considered to be a constant with varying Nb-doping concentration due to their similar composition and no phase transition. In this case, the oxygen permeation flux was then mainly determined by the oxygen vacancy concentration. Since Nb took 5+ valence state at the B-site, the increase in Nb-doping content led to a decrease of oxygen vacancy concentration, it then well explains the decrease in permeation flux with increase Nb content. For B-site Nb-doped $SrCoO_x$ ($SrCo_{1-y}Nb_yO_{3-\delta}$), its phase stability under nitrogen atmosphere increased steadily with Nb concentration until a pure perovskite phase was sustained at $y \geq 0.1$. At $y \leq 0.1$, the oxygen permeation flux was mainly determined by the phase structure of the oxide, the increase in oxygen permeation flux with Nb-doping amount was attributed to the increase of the phase stability under a nitrogen atmosphere. At $y \geq 0.1$, the perovskite structure was sustained and the permeation flux was mainly determined by the oxygen vacancy concentration. The increase in Nb-doping content resulted in a decrease in oxygen vacancy concentration due to its higher valence state (5+) when compared to cobalt (3+/4+). This explains the decrease in permeation flux with the further increase of Nb-doping content at $y \geq 0.1$. The optimal B-site Nb-doping concentration is $y = 0.1$. It should be noted that Fig. 6a also reveals some unusual permeation behavior of membranes with $x = 0.025$ and 0.05. At temperatures lower than 800 °C, the permeation flux through the membrane with $x = 0.05$ is higher than for $x = 0.025$, whilst for temperatures above 800 °C, an opposite situation is observed. At this stage, this unusual phenomenon cannot be explained.

Among all the Nb-doped $SrCoO_x$ oxides, $SrCo_{0.9}Nb_{0.1}O_{3-\delta}$ shows the highest permeation flux and favorable phase stability under oxygen separation conditions. It delivered a permeation flux as high as ~3.5 m cm^{-2} min^{-1} [STP] at 900 °C under air/helium gradient, which is one of the best values in the oxygen permeation fluxes for various oxygen semi-permeable ceramic membranes under similar operation conditions ever reported up to now. Double-site Nb-doped $SrCoO_x$ with the composition of $Nb_{0.025}Sr_{0.975}Co_{0.975}Nb_{0.025}O_{3-\delta}$ showed the second highest permeation flux of 2.7 ml cm^{-2} min^{-1} [STP] at 900 °C. Both $Nb_{0.025}Sr_{0.975}Co_{0.975}Nb_{0.025}O_{3-\delta}$ and $SrCo_{0.9}Nb_{0.1}O_{3-\delta}$ also demonstrated favorable phase stability under oxygen permeation conditions. Therefore they are highly promising as materials of ceramic membrane for oxygen separation from air.

4. Conclusions

Niobium was successfully doped into the A-site, B-site, or simultaneously A and B double sites of the parent $SrCoO_x$ oxide. A cubic perovskite structure was obtained in air when the niobium doping range was $x = 0.025$–0.2, $y = 0.025$–0.2 and $z = 0.025$–0.1 for A-site doping ($Nb_xSr_{1-x}CoO_{3-\delta}$), B-site doping ($SrCo_{1-y}Nb_yO_{3-\delta}$) and double-site doping ($Nb_zSr_{1-z}Co_{1-z}Nb_zO_{3-\delta}$), respectively. The A-site doping, however, was not able to stabilize the cubic structure in a lower oxygen containing or reducing atmosphere like nitrogen. As to

B-site doping, the cubic perovskite was sustained in nitrogen only at $y \geq 0.1$. Double-site doping is the most effective way to stabilize the cubic structure in nitrogen where no phase transition occurs at $z = 0.025$–0.1. The stabilization of cubic perovskite structure resulted in a sharp increase of electrical conductivity and oxygen permeation fluxes. A maximum conductivity of $\sim$450 S cm^{-1} was achieved for $SrCo_{0.975}Nb_{0.025}O_{3-\delta}$ at 300 °C in air. However, niobium acted as a hopping block for electrons in cubic perovskite structure, consequently, a decrease in electrical conductivity with continually increasing Nb-doping content was observed. Ceramic membranes of $Nb_{0.025}Sr_{0.975}Co_{0.975}Nb_{0.025}$ and $SrCo_{0.9}Nb_{0.1}O_{3-\delta}$ show the highest permeation fluxes among the Nb-doped series of $SrCoO_x$ oxide with values of 3.5 and 2.7 ml cm^{-2} min^{-1}, respectively. They are promising candidates as materials for air-separation membranes.

Acknowledgements

This work was supported by the National Science Research Foundation of China contract Nos. 20701020 and 20703024, Fok Ying Tung Education Foundation No. 111073. Dr. Liu acknowledges the ARC fellowship provided by the Australian Research Council.

References

[1] Y. Teraoka, H.M. Zhang, S. Furukawa, N. Yamazoe, Chem. Lett. 11 (1985) 1743.
[2] Z.P. Shao, W.S. Yang, Y. Cong, H. Dong, J.H. Tong, G.X. Xiong, J. Membr. Sci. 172 (2000) 177.
[3] L.-W. Tai, M.M. Nasrallah, H.U. Anderson, D.M. Sparlin, S.R. Sehlin, Solid State Ionics 76 (1995) 259.
[4] H.H. Wang, R. Wang, D.T. Liang, W.S. Yang, J. Membr. Sci. 243 (2004) 405.
[5] L. Qiu, T.H. Lee, L.-M. Liu, Y.L. Yang, A.J. Jacobson, Solid State Ionics 76 (1995) 321.
[6] H.H. Wang, Y. Cong, W.S. Yang, Catal. Today 82 (2003) 157.
[7] Z.P. Shao, G.X. Xiong, H. Dong, W.S. Yang, L.W. Lin, Sep. Purif. Technol. 25 (2001) 97.
[8] P.J. Gellings, H.J.M. Bouwmeester, Catal. Today 58 (2000) 1.
[9] P.Y. Zeng, R. Ran, Z.H. Chen, H.X. Gu, Z.P. Shao, S.M. Liu, AIChE 53 (2007) 12.
[10] Z.H. Chen, R. Ran, W. Zhou, Z.P. Shao, S.M. Liu, Electrochim. Acta 52 (2007) 7343.
[11] M.A. Peña, J.L.G. Fierro, Chem. Rev. 101 (2001) 1981.
[12] Z.P. Shao, S.M. Haile, Nature 431 (2004) 170.
[13] B.C.H. Steele, A. Heinzel, Nature 414 (2001) 345.
[14] T. Hibino, A. Hashinmoto, T. Inoue, J. Tokuno, S. Yoshida, M. Sano, Science 288 (2000) 2031.
[15] S.B. Adler, Chem. Rev. 104 (2004) 4791.
[16] N.P. Brandon, S. Skinner, B.C.H. Steel, Annu. Rev. Mater. Sci. 33 (2003) 183.
[17] S. Mclntosh, R.J. Gorte, Chem. Rev. 104 (2004) 4845.
[18] P.Y. Zeng, Z.H. Chen, W. Zhou, H.X. Gu, Z.P. Shao, S.M. Liu, J. Membr. Sci. 291 (2007) 148.
[19] T. Nagai, W. Ito, T. Sakon, Solid State Ionics 177 (2007) 3433.
[20] K. Zhang, R. Ran, L. Ge, Z.P. Shao, W.Q. Jin, N.P. Xu, J. Alloys Compd. 474 (2008) 477.
[21] K. Zhang, R. Ran, L. Ge, Z.P. Shao, W.Q. Jin, N.P. Xu, J. Membr. Sci. 323 (2008) 436.
[22] H. Kruidhof, H.J.M. Bouwmeester, R.H.E. van Doorn, A.J. Burggraaf, Solid State Ionics 63 (1993) 816.
[23] T.S. Zhang, J. Ma, L.B. Kong, S.H. Chan, J.A. Kilner, Solid State Ionics 170 (2007) 209.
[24] R.D. Shannon, C.T. Prewitt, Acta Crystallogr. Sect. B 25 (1969) 925.
[25] C. Zerner, Phys. Rev. 82 (1952) 403.